Geophysical Prospecting, 2003, **51**, 183–193

A quantitative study on the use of converted waves for sub-basalt imaging

Peter Hanssen,[1]* Anton Ziolkowski[2] and Xiang-Yang Li[1]

[1]*British Geological Survey, Murchison House, West Mains Road, Edinburgh EH9 3LA, and* [2]*Department of Geology and Geophysics, University of Edinburgh, West Mains Road, Edinburgh EH9 3JW, UK*

Received June 2002, revision accepted August 2002

ABSTRACT

The idea of imaging beneath a high-velocity layer using converted waves has been popular since 1990. Because these wave types have their maximum amplitudes at mid- to far-offsets, the search for pure P-waves at the highly multiple-contaminated near-offsets can be avoided. For the Atlantic Margin, with buried thin-layered basalts, our quantitative study shows that the initial single-layered approach is not viable. Even in an unrealistic ideal geological setting, the amplitude of the symmetrical PSP-mode is far too weak to be recognized on towed streamer data. Furthermore, in the far-offset window, where locally converted waves have their strongest amplitudes, there is a multitude of other reflections, refractions and interbedded multiples, which have similar moveouts and, often, higher amplitudes. Without the removal of these events, a reliable image of the subsurface cannot be produced. We show that even if this problem were solved, it would be far easier to use the P-wave reflection from beneath the basalt at near-offsets. Our study shows that this wave type is by far the strongest response. A borehole-derived model using a thin-layered basalt sequence reveals that the strongest locally converted wave has an asymmetrical path and is 10 times weaker. All our results indicate that the pure P-modes provide the best chance of imaging sub-basalt sedimentary interfaces.

INTRODUCTION

Large areas of the northeast Atlantic Margin are covered by Early Cenozoic flood basalts extruded by igneous centres. They may cover hydrocarbon reservoirs, as these have been found outside the basalt-covered area near the Shetlands (Fig. 1). The underlying Mesozoic and Palaeozoic sediments, which have been shown to function as source and reservoir rocks (Stoker, Hitchen and Graham 1993), could not hitherto be imaged with seismic waves, mainly because the high seismic velocities of the overlying basalts created severe multiple reflections.

Studies of refracted waves at far-offsets in basalt-covered areas of the northeast Atlantic Margin date back to the 1960s (Pálmason 1965; Scrutton 1970, 1972). They resolve only major high-velocity contrasts beneath basalt, and not the many subtle reflections within the underlying sediments. Nevertheless, refraction profiles might be useful to determine the thickness of the underlying sedimentary package between the base of the basalts and the basement (Jarchow, Catchings and Lutter 1994; Shipp, Singh and Barton 1997; Richardson *et al.* 1999). In an offshore situation this can be achieved using two boats (White *et al.* 1982; Frühn *et al.* 1998) or ocean-bottom seismometers (Samson, Barton and Karwatowski 1995; Hughes, Barton and Harrison 1998; Kodaira *et al.* 1998).

To image sedimentary interfaces beneath a high-velocity layer, Purnel *et al.* (1990) suggested that locally converted waves should be used instead of pure P-waves. This approach was first examined for basalt-covered areas by Li and MacBeth (1996). They proposed using a less multiple-disturbed, converted wavetrain at offsets beyond the first

*E-mail: hanssen@bgs.ac.uk

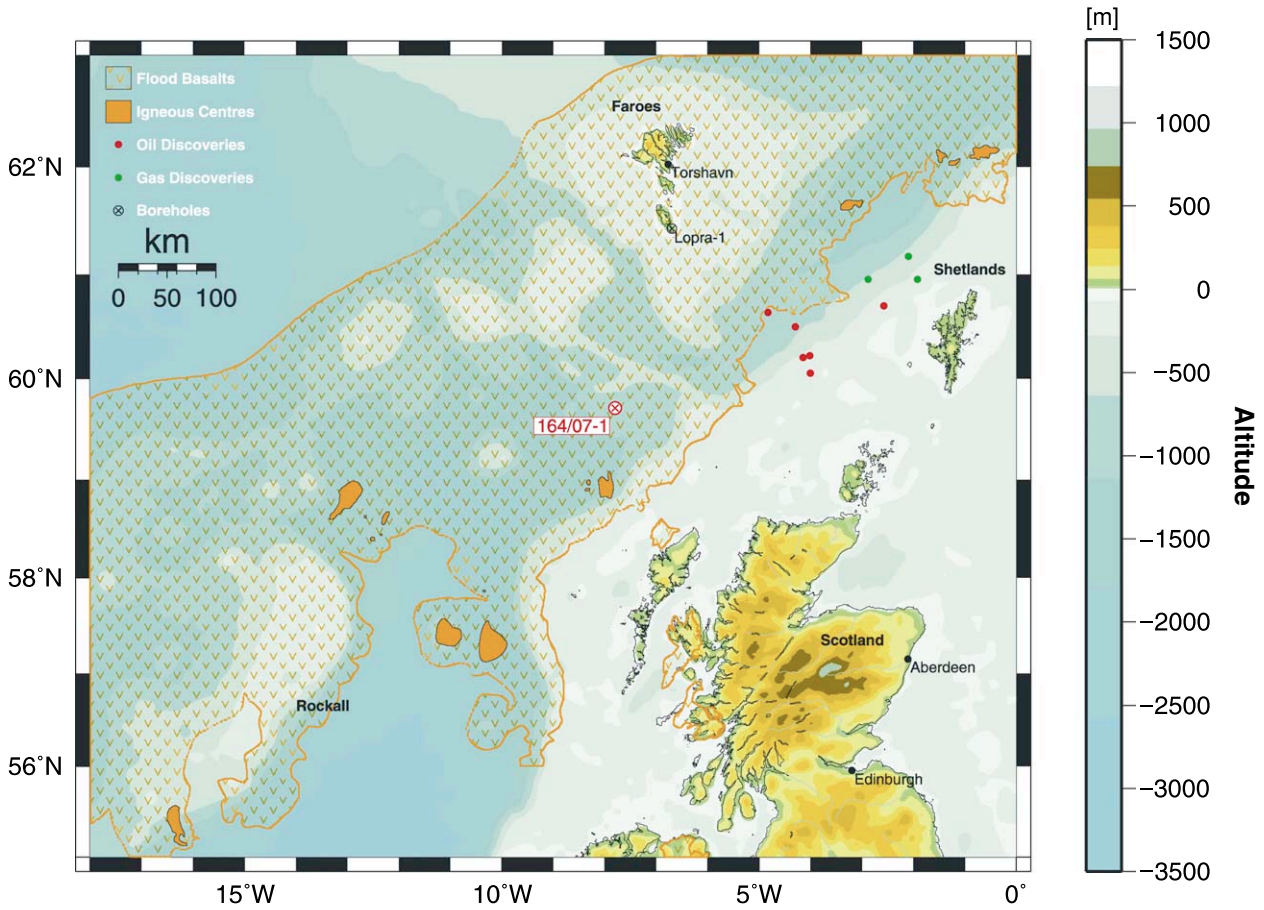

Figure 1 Basalt-covered areas of the northeast Atlantic Margin showing the location of borehole 164/07-1 and hydrocarbon discoveries in the Faeroe-Shetland Basin.

break of the sea-bed reflection (Li *et al*. 1998). Unfortunately this wavetrain will be disturbed by refracted multiples (Longshaw, Sunderland and Horn 1998), other reflections and interbed multiples (Hanssen, Ziolkowski and Li 1998).

We examine the possibility of recording locally converted shear waves. Starting with a single, thin and homogeneous layer, we increase the complexity of the basalt sequence and use borehole data of alternating basalts and sediments to observe the effects on converted waves. To study changes in the converted-wave responses along the northeast Atlantic Margin, our models vary from intermediate to deep waters and from 200 to 800 m in basalt thickness.

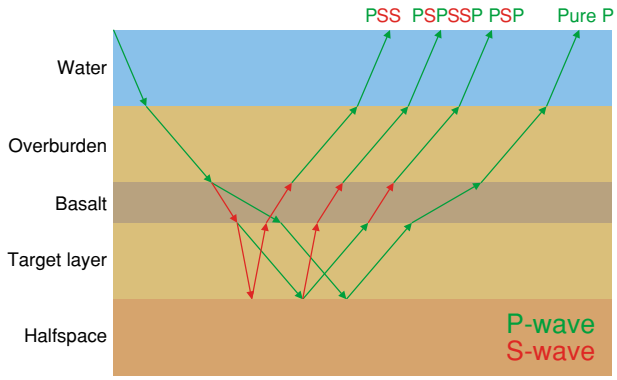

Figure 2 Schematic diagram of wave paths for the main reflected waves through a single-layered basalt for a streamer recording.

SINGLE-LAYERED BASALT

Figure 2 shows possible conversions from P- to S-wave or from S- to P-wave at each of the interfaces between low-velocity and high-velocity layers (here, sediments overlying basalt or sand below basalt). The PSP-wave has S-modes only inside the basalt and the PSS-wave contains only S-modes below the top of the basalt. Both locally converted waves are symmetrical (three-letter notation) and could be

processed with standard methods. Other reflections with asymmetrical paths were considered in our study, but only the PSPSSP-mode showed significant amplitudes for a single-layered basalt.

To investigate in detail the behaviour of converted waves in basalt-covered areas, we first use a simple, horizontally layered, geological model (Fig. 3, top left), which is partly based on seismic results near the Rockall Bank (Li and MacBeth 1996). Two sandstone units form the target interface and are overlain by a homogeneous and isotropic basalt layer, which is itself overlain by a sediment unit and the water column. In this 'ideal model', the shear-wave velocity V_S of the basalt is close or equal to the primary-wave velocity V_P of the overlying and underlying rocks. This high

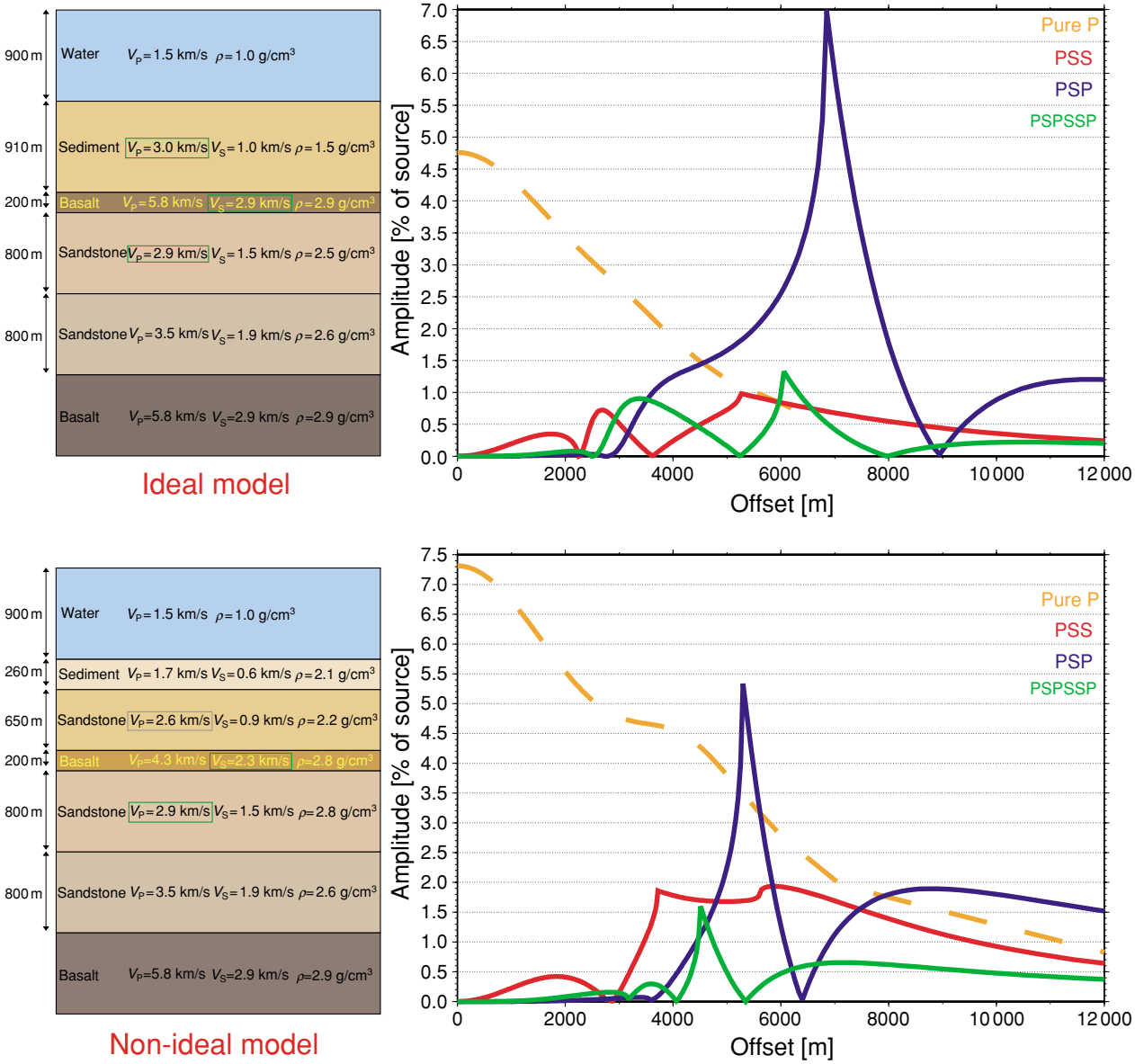

Figure 3 Simple, isotropic, horizontally stratified models for an offshore sub-basalt area, and effective reflection coefficients for the four strongest reflections recorded at the sea-surface from the sandstone–sandstone target interface as a function of offset and percentage of source amplitude. Top: 'ideal model' using an idealistic velocity match between the S-wave velocity of the basalt and overlying and underlying sedimentary P-wave velocities. Bottom: 'non-ideal' model with a slight mismatch of the S-wave velocity of the basalt and overlying and underlying sedimentary P-wave velocities.

P-wave velocity-contrast leads to high conversion coefficients at the top and the bottom interface of the basalt.

For full understanding of the transmission and reflection process through basaltic layers, the effective reflection coefficients have to be considered. The effective reflection coefficient of a target layer consists of all transmission coefficients at the interfaces above for the downgoing and upgoing path in layered media, and the reflection coefficient at the target interface. This can be calculated, using the exact formula for horizontal layered media of Aki and Richards (1980), with a plane wave and not accounting for spherical divergence. We calculated the effective reflection coefficients using all possible wave paths of target reflections for the above model. Figure 3 (top right) shows the resulting effective reflection coefficients of the four target waves with the highest amplitude. The coefficients are normalized by the source amplitude and their moduli are plotted as a function of offset. Owing to the high velocity-contrast at the top-basalt interface, the pure P-wave is refracted shortly after the 6 km offset and only shear modes are transmitted beyond this point. Locally converted S-waves are detectable up to 12 km. Furthermore, it can be seen that the PSP-wave, with S-waves only inside the basalt, has the highest amplitude at offsets around 7 km. The amplitude is about 7% of the source amplitude and that of the second strongest converted wave is only 1.9% of the source amplitude. A polarity reversal occurs when a curve touches the zero-amplitude value. This happens once for PSP at far-offsets but not for PSS, which consists only of S-waves below the top of the basalt. The wave with an asymmetrical raypath (PSPSSP) has a similar amplitude to the PSS-mode but experiences three phase changes (or polarity reversals in the time domain), making it more difficult to trace at mid- to far-offsets.

In contrast to the 'ideal model', the velocities of the second 'non-ideal model' (Fig. 3, bottom left) do not match perfectly, which is what we would expect in most cases in the real world. Additionally, the sediment overlying the basalt is split into two parts and has lower velocities and higher densities than the first model (Fig. 3, top left). The basalt layer also has lower velocities and a slightly lower density. The velocities governing the PSP-conversion through the basalt show a greater difference and range from $V_P = 2.6$ km/s to $V_S = 2.3$ km/s and to $V_P = 2.9$ km/s. The effective reflection coefficients for this 'non-ideal model' show an increase in the P-wave amplitude at near-offsets, as shown in Fig. 3 (bottom right). Because the P-wave is not yet refracted at mid-range offsets but is still transmitted through the basalt, we observe a decrease in the PSP-amplitude when compared with the

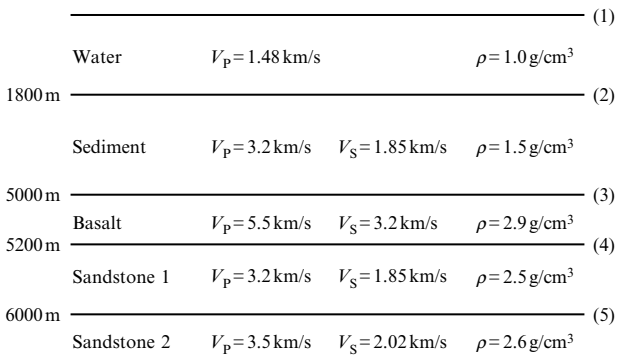

Figure 4 Initial offshore model with an interbedded high-velocity layer for the calculation of effective reflection coefficients with varying velocity values of the basalt.

'ideal-model' calculations shown in Fig. 3 (top right). The more realistic model shows that the P-wave is present throughout the 12 km offset because of the lower P-wave velocity contrast compared with the 'ideal model'. Except for a sharp peak of the PSP-mode around 5500 m, the pure P-wave is the strongest wave up to about 8000 m offset, compared with 4000 m for the 'ideal model'. The wave with S-waves only through the basalt (PSP) has the highest amplitude from about 8000 m onwards. In contrast to the 'ideal model', the PSS-mode is more likely to be recognized and again has no polarity reversals at far-offsets, unlike the PSP-mode, which has one at about 6500 m. The asymmetrical PSPSSP-mode shows the most polarity reversals and is the weakest of the four target reflections.

To examine the three main target waves (P, PSP, PSS) more closely, the effective reflection coefficients were again calculated using the simple model of Fig. 4. The model is based on a horizontally layered and isotropic model from the Rockall Trough, which includes a deep-water layer of 1.8 km. A basaltic layer of 200 m thickness is overlain and underlain by sediments, which initially have P-wave velocities equal to the S-wave velocity of the basalt. Below this, a half-space forms the target interface (5) at 6 km depth with the sediment layer below the basalt. The density of the high-velocity layer was kept constant and the internal velocity ratio followed $V_P/V_S = 3^{1/2}$. To compare the amplitude behaviour of the reflected modes, the velocity ratio between the basaltic S-wave and the sedimentary P-waves (V_{S2}/V_{P1}) was varied between 0.6 and 1.4.

The effective reflection coefficients for the wave with only S-modes below the top of the basalt (PSS) is shown in Fig. 5 (right) as a function of velocity ratio and angle. The calculation reveals two maxima in amplitude for this kind of wave

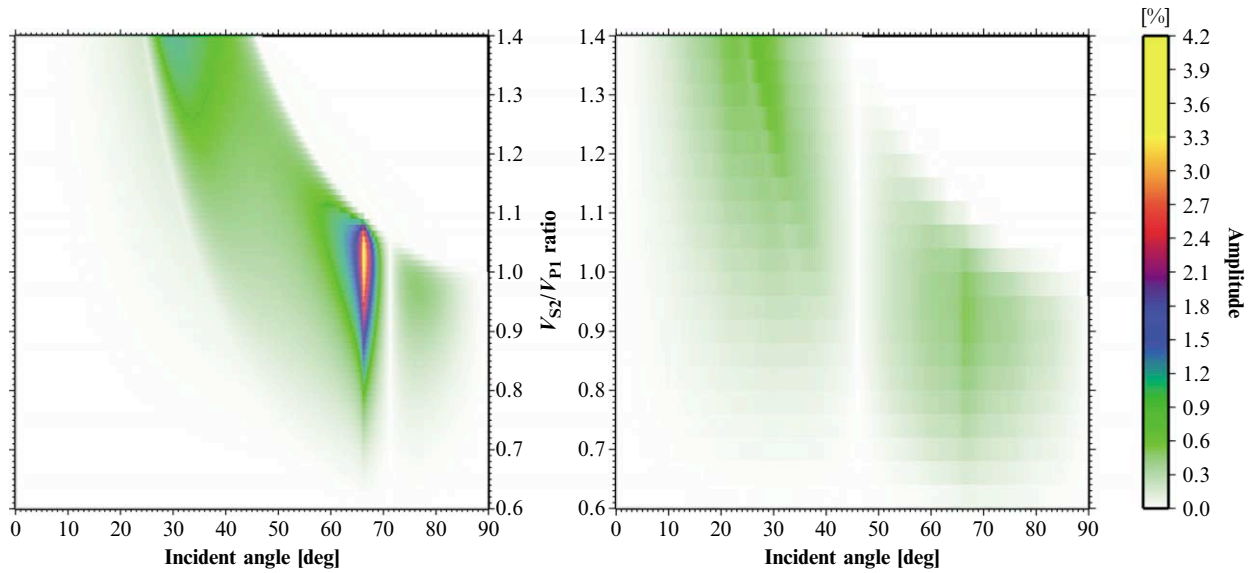

Figure 5 Effective reflection coefficients as a function of incident angle and a varying ratio of the S-wave velocity of the basalt (V_{S2}) to P-wave velocities of the overlying and underlying rocks (V_{P1}). Left: for the PSP-mode; right: for the PSS-mode.

mode. If the P-wave velocities of the sediments are greater than or equal to the S-wave velocity of the basalt, i.e., $V_{S2}/V_{P1} \leq 1$, we observe a maximum at far-offsets around an incident angle of 66° or 5.1 km offset. For ratios above 1, this maximum decreases and the maximum amplitude for the PSS-mode can be recorded at mid-offsets with incident angles around 20–30° (0.9–1.5 km). Overall, the amplitude does not exceed 1% of the source amplitude.

Figure 5 (left) shows the effective reflection coefficient for the PSP-mode as a function of the V_{S2}/V_{P1} ratio and the incident angle. It shows a distinctive maximum around a velocity ratio of 1. This corresponds to the original model where the P-wave velocities above and below the basalt equal the S-wave velocity inside the basaltic layer. The maximum is also sharply restricted to an incident angle of 66° or 7.3 km offset. As for the PSS-mode, the PSP-mode can be recorded only at large offsets. Furthermore, the maximum amplitude of this locally converted shear wave reaches 4.1% of the source amplitude, which is four times stronger than the maximum amplitude of the PSS-mode. By contrast, the peak of the maximum amplitude of the PSP-mode is very narrow and can be observed only in ideal circumstances, compared with the wider amplitude peak of the PSS-wave. Figure 6 shows the effective reflection coefficient of the PSP-mode compared with the pure P-wave reflection of the sub-basalt target. The amplitude of the P-wave at near-offsets exceeds the amplitude of the locally converted wave, not only where the S- and P-wave velocities do not match but also at a ratio of $V_{S2}/V_{P1} = 1$. We observe a narrow band of maximum amplitude for the PSP-mode at large incident angles, compared with the almost constant amplitude of the P-wave for small incident angles. Furthermore, it shows that the P-wave amplitude reaches values at least double the size of that of the PSP-wave. This is the case not only when the S-wave velocity of the basalt is lower than the P-wave velocity of the overlying and underlying layers ($V_{S2}/V_{P1} < 1$), but also when the S-wave velocity of the basalt is higher than the overlying and underlying P-wave velocities ($V_{S2}/V_{P1} > 1$).

Using the 'ideal model' of Fig. 3 (top left), we calculated a full-waveform seismogram using a Ricker wavelet with a centre frequency of 25 Hz. This and the following synthetic seismograms were calculated using the full-waveform modelling package Osiris by Ødegaard (Vilmann, Gerstoft and Krenk 1998). Figure 7 shows the proposed less-disturbed wavetrain (Li and MacBeth 1996) between 5 km and 12 km offsets, using the sea-bed and top-basalt reflections (yellow-dashed traveltime curves) as mute borders. On top of the synthetic seismogram, the traveltime curves of the three main locally converted waves are plotted with additional traveltime curves for some other reflections (red-dotted), refracted waves (green-dotted) and interbed multiples (turquoise-dashed). We observe reflections, which follow the PSP and PSS trend, but the moveouts of these waves are very similar to those of interbed multiples. Even using a simple model like this, it is impossible to distinguish between multiples and target reflections. The asymmetrical PSPSSP-mode is too

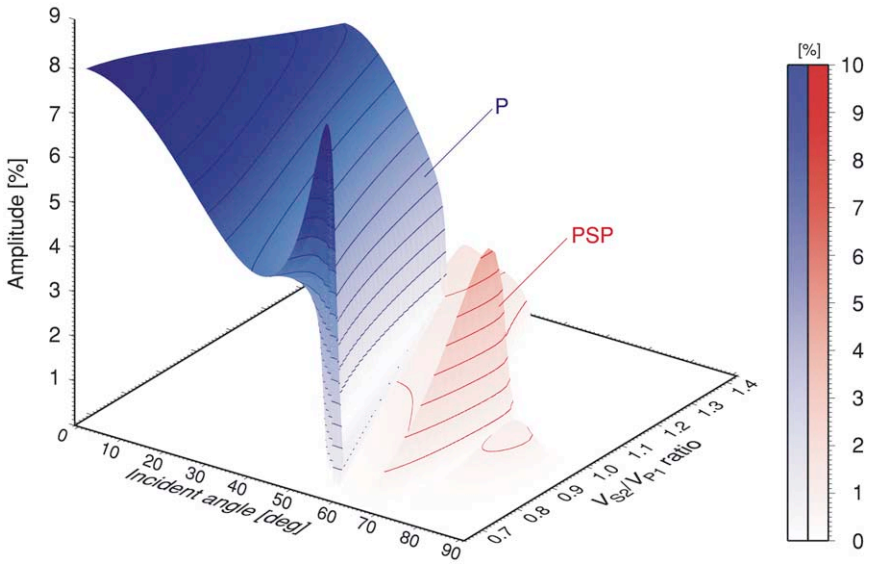

Figure 6 Effective reflection coefficients for the pure P-wave and the PSP-mode as a function of incident angle and a varying ratio of the S-wave velocity of the basalt (V_{S2}) to P-wave velocities of the overlying and underlying rocks (V_{P1}).

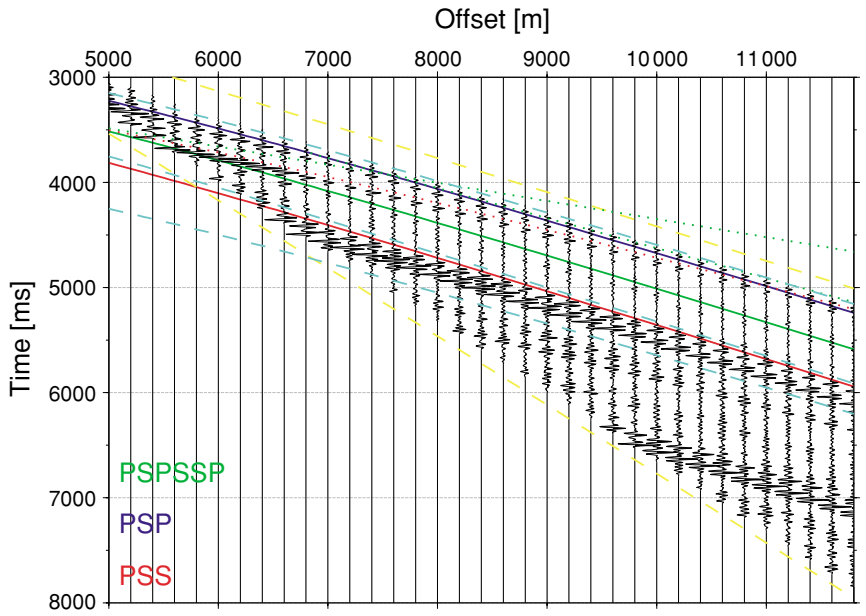

Figure 7 Synthetic seismogram showing the wavetrain for the 'ideal model' with offsets between 5 km and 12 km including traveltime curves for the three locally converted waves, sea-bed and top-basalt P-wave reflections (yellow-dashed), other reflections (red-dotted), refractions (green-dotted) and some multiples (turquoise-dashed) with similar moveouts.

weak even to show up on the noise-free synthetic seismogram. In addition, other events from above the target, refracted waves and their multiples, appear in this window with similar moveouts.

Even in this noise-free case, where the model is extremely simple and known fully, we cannot separate the genuine converted-wave target reflections from these unwanted reflections and multiples. In real, noisy data, where the earth is much more complex, we believe this separation would be impossible.

MULTILAYERED BASALT

We know that the assumption of a single-layered basalt is not true for most areas along the North Atlantic Margin (Planke, Alvestad and Eldholm 1999). Therefore we constructed a more realistic multilayered basalt model, based on acoustic-log data from Conoco's borehole 164/07-1 (see Fig. 1). We placed 800 m of the recorded basalt P-wave velocities beneath 600 m of sediment and 425 m of water (Fig. 8). Two sediment layers were inserted beneath the basalt. The upper

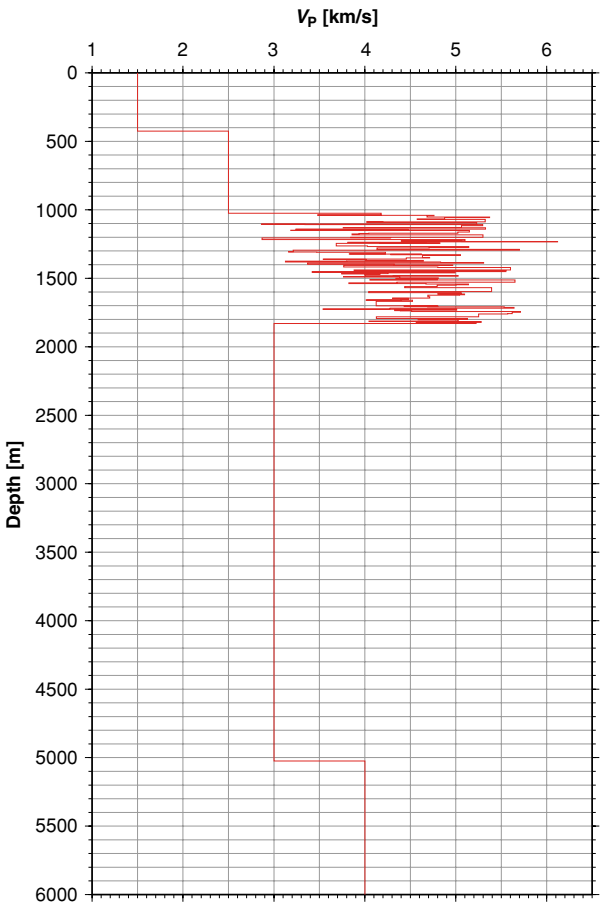

Figure 8 P-wave velocity model using part of the acoustic log of borehole 164/07-1 through basalt and one deep sub-basalt reflector.

one ($V_P = 3000$ m/s and $V_S = 1732$ m/s) and the lower one ($V_P = 4000$ m/s and $V_S = 2309$ m/s) formed a sub-basalt target interface with a P-wave velocity difference of 1000 m/s at 5025 m depth: deep enough to avoid overlying basalt reflections. Within the basaltic interval the average P-wave velocity is about 4500 m/s and varies rapidly between 2300 m/s and 6400 m/s. Also the density in this zone shows abrupt changes between 1.5 g/cm^3 and 2.9 g/cm^3. We resampled the original P-wave velocity and density at 2 m intervals to incorporate most of the thin sedimentary layers between basalt flows and to consider velocity gradients within the different basalt layers. The S-wave velocity was calculated for an isotropic model using a V_P/V_S ratio of 1.8.

The synthetic seismogram using a delayed three-loop Ricker wavelet with a centre frequency of 35 Hz is shown in Fig. 9 (left). The pure P-wave reflection from beneath the basalt is not visible due to the sea-surface-related multiple contaminations. If we remove the sea-surface from our model, the resulting seismogram (Fig. 9, right) clearly shows the pure P-wave reflection from the target. For an area with homogeneous, thinly layered basalts, only the free-surface multiples hide deep sub-basalt reflections. However, if we moved our target interface just 100 m beneath the basalt sequence, the target reflection would also be obscured by internal basalt multiples and mode-converted basalt waves around 1.5 s two-way traveltime.

In order to examine the response of the sub-basalt target only, we calculated the synthetic seismogram for the original model again, but without the deepest layer. This removes the target interface and leaves only a sedimentary half-space below the basalt. Subtracting this result from the original seismograms, one with and one without the sea-surface, produces the seismograms shown in Fig. 10. The traveltime curves for the strongest reflections are plotted in red. PS-wave stands for only P-modes down to the target, only S-modes from the target to the sea-bed and a P-wave through the water to the hydrophones. The PSSSSS-wave runs in P-mode down to the top of the basalt, from thereon only in S-mode until it changes to P-mode on the way through the water to the hydrophones. The shear wave contains only S-modes below the sea-bed and P-modes inside the water. The calculations show that even without sea-surface multiples and knowledge of the model, none of the converted target waves can be traced except the pure P-wave.

Figure 11 (right) shows the effective reflection coefficients for the six strongest sub-basalt responses and two interbed multiples. As the synthetic seismograms showed, the pure P-wave is by far the strongest mode to be expected in streamer data. Its amplitude has a maximum at near-offsets of about 0.7% of the source amplitude. The calculation confirms the findings from Fig. 10, that even interbed multiples are stronger than any of the converted waves. Moreover this is not only at near-offsets but applies over the whole measured offset range. Figure 11 (left) shows the converted waves in detail. The common PS-wave has the strongest amplitude around 2700 m, which is at least 20 times weaker than the pure P-wave. The second strongest of these converted waves is the 'shear wave'. This shows that ocean-bottom recordings and shooting might be successful in recording other strong responses from beneath the basalt (Hanssen, Li and Ziolkowski 2000). Figure 11 also confirms that the PSP-mode has a very weak amplitude if the S-wave velocities of the basalt layers do not match the overlying and underlying P-wave velocities. The calculation confirms also that the PSS-mode is less sensitive to a velocity match. Owing to the complex velocity structure of the basalt sequence, we find a new

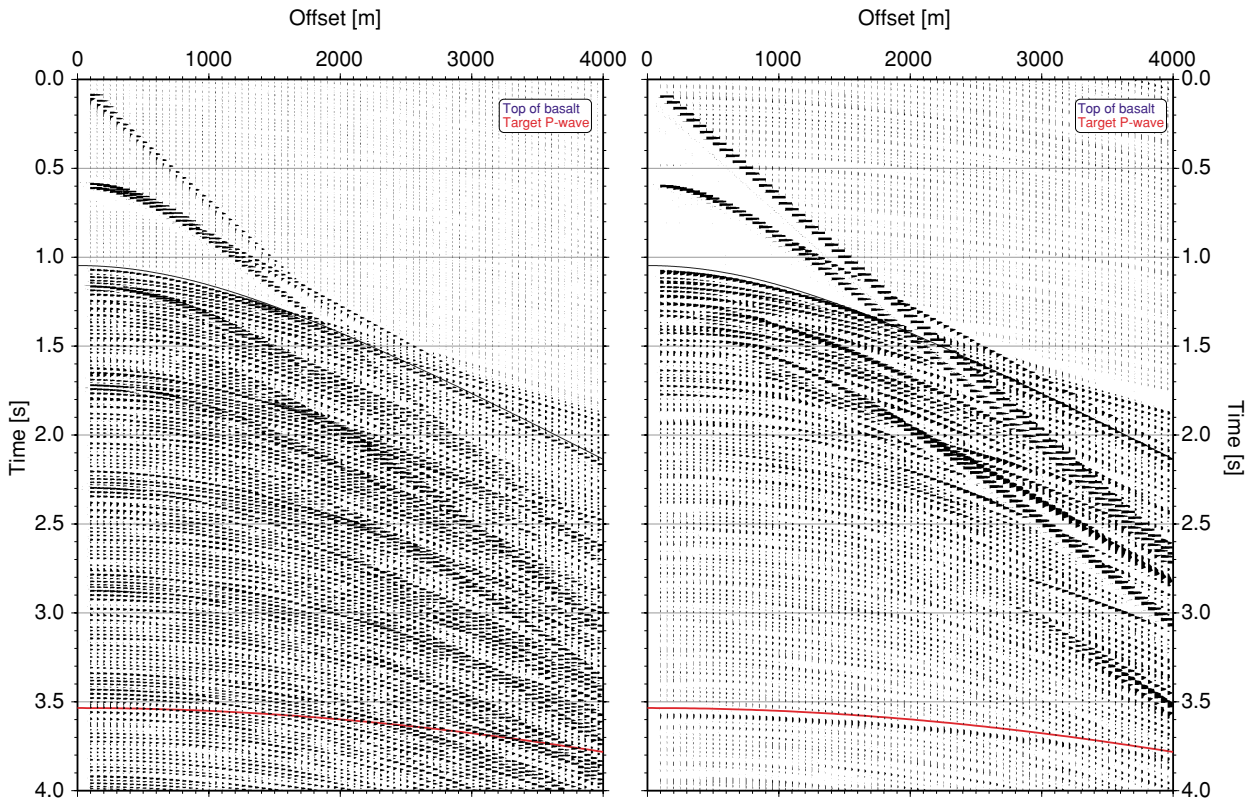

Figure 9 Synthetic seismograms for the multilayered basalt model of Fig. 8, showing P-wave traveltime curves for reflections from the top of the basalt (blue) and the sub-basalt interface (red). Left: including sea-surface; right: without sea-surface.

locally converted wave with amplitudes similar to the PSS-wave. The PSSSSS-wave has amplitudes higher than the PSS-mode but would probably improve when measured on the sea-bed. However, handling this type of mode would require non-standard processing due to its asymmetrical travelpath.

Another striking difference from the results of the models with one solid basalt layer (Fig. 3) is the shift of higher-amplitude reflections to shorter offsets when using the multilayered model from the seismic borehole data. The five most energetic target reflections have their maximum amplitudes between 2100 and 2700 m and could be recorded with a standard 6 km streamer. The exact offset for the maximum amplitude peak is of course dependent on the depth of the different layers and also on the velocities, and is especially sensitive to the velocities of the basalt layers.

The transmission through the multilayered basalt sequence also dramatically changes the amplitude behaviour of all converted waves over offset. Owing to the varying thicknesses and velocities of the thin layers and the presence of numerous high-contrast interfaces, the amplitudes are well behaved and do not show the frequent polarity reversals that are observed with single-layered models (Fig. 3). At far-offsets beyond 8000 m, the converted waves are either refracted (PS-wave) or their amplitudes become negligible.

DISCUSSION AND CONCLUSION

Our study of full-waveform synthetic seismograms and effective reflection coefficients shows that the pure P-wave is better suited to imaging sedimentary interfaces beneath a high-velocity basalt sequence than any locally converted wave. Even in an ideal case with one homogeneous basalt layer, where the S-wave velocity exactly matches the overlying and underlying P-wave velocities, the pure P-wave reflection contains more energy than any other mode. Additionally, the weak locally converted waves are masked at far-offsets by other reflections, refractions and interbed multiples with similar moveouts. For a single-layered basalt model, the symmetrical PSP-mode is the strongest converted reflection at far-offsets and the PSS-wave is the second strongest. Using a more realistic model based on an acoustic log reveals that the PSP-wave reflection has negligible amplitudes. This is due to the thinly

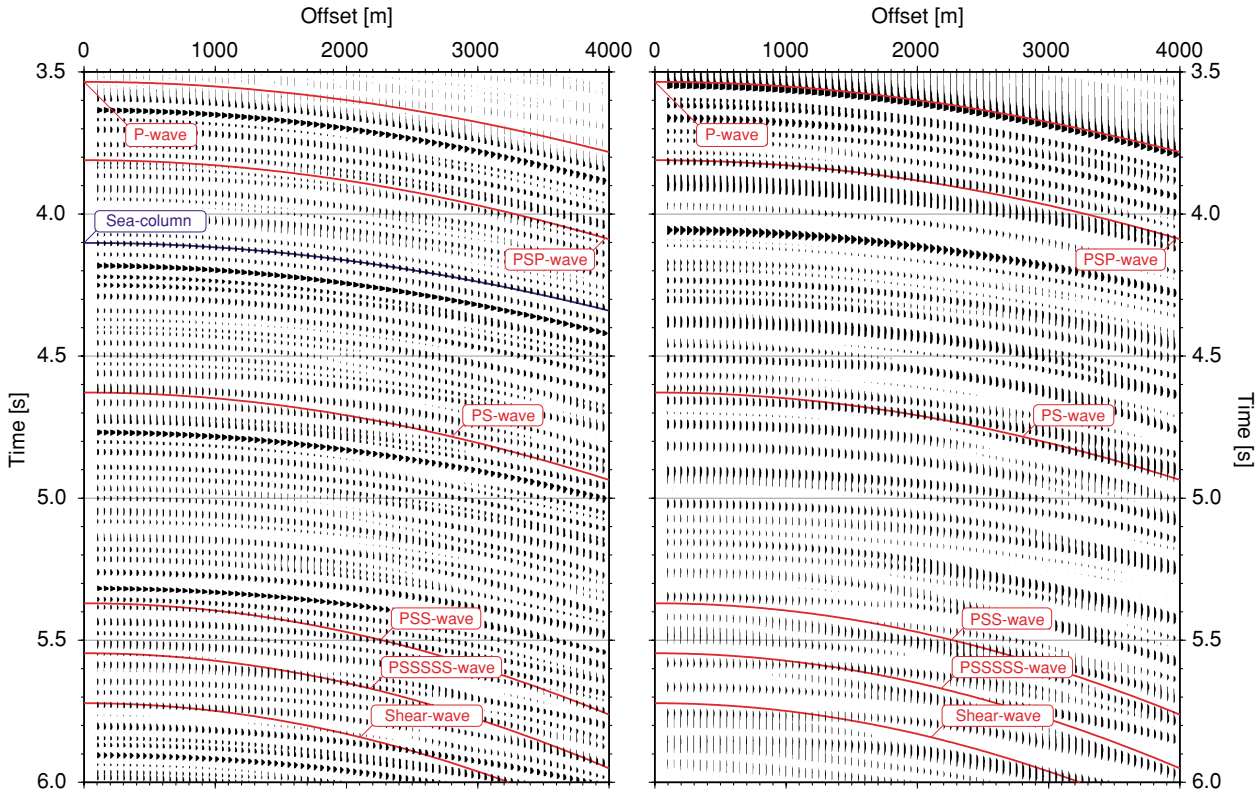

Figure 10 Shot gathers showing the seismic response of the sub-basalt interface only (see text for details) with plotted traveltime curves for associated target reflections. Left: including sea-surface; right: without sea-surface.

layered structure of basalt sequences and the resulting mismatch of S- and P-wave velocities. In this case, the PSS-wave transports more energy back from a sub-basalt target than the PSP-mode. Also, the strongest locally converted wave becomes a PSSSSS-wave with an asymmetrical path. Owing to the upgoing S-mode at the sea-bed of this wave, an ocean-bottom recording would be favourable. In the case of an OBC/S recording, we can expect additional strong amplitudes from PS-waves at mid-offsets. A pure shear wave might be recorded using an appropriate sea-bed source. If it is planned to use locally converted modes to image beneath basalts, not only must the sea-surface-related multiples be removed but also interbed multiples. If this can be reliably performed for streamer data at mid- to far-offsets, then it would be preferable to use just the pure P-waves at near-offsets because their amplitudes are a multiple of 10 times stronger than the amplitude of any converted wave through a thinly layered basalt sequence. Data from other boreholes in basalt-covered areas show similar layered basalt structures as they are formed by single lava flows. It is therefore highly unlikely that matching velocities, which allow the use of Purnel *et al.*'s (1990) idea, will be observed. The only occasion to observe locally converted waves will probably be in the case of an 'ideal-model' situation such as a single basalt layer or a single sill. Even then, OBC/S or VSP recordings would be required to enhance the weak, converted reflections. The amplitude response from beneath a thinly layered sequence increases with decreasing frequency (see also Ziolkowski *et al.* 2003). In addition, absorption will influence the effective reflection coefficients, but in general both effects do influence all wave types, more or less equally.

ACKNOWLEDGEMENTS

We thank Jonathan Scorer, Conoco (UK) Ltd and tranche partners for making the borehole data available to us and for permission to publish the data. P.H. and X.-Y.L. are funded by the sponsors of the Edinburgh Anisotropy Project. This work is published with the approval of the Director of the British Geological Survey and the EAP sponsors:

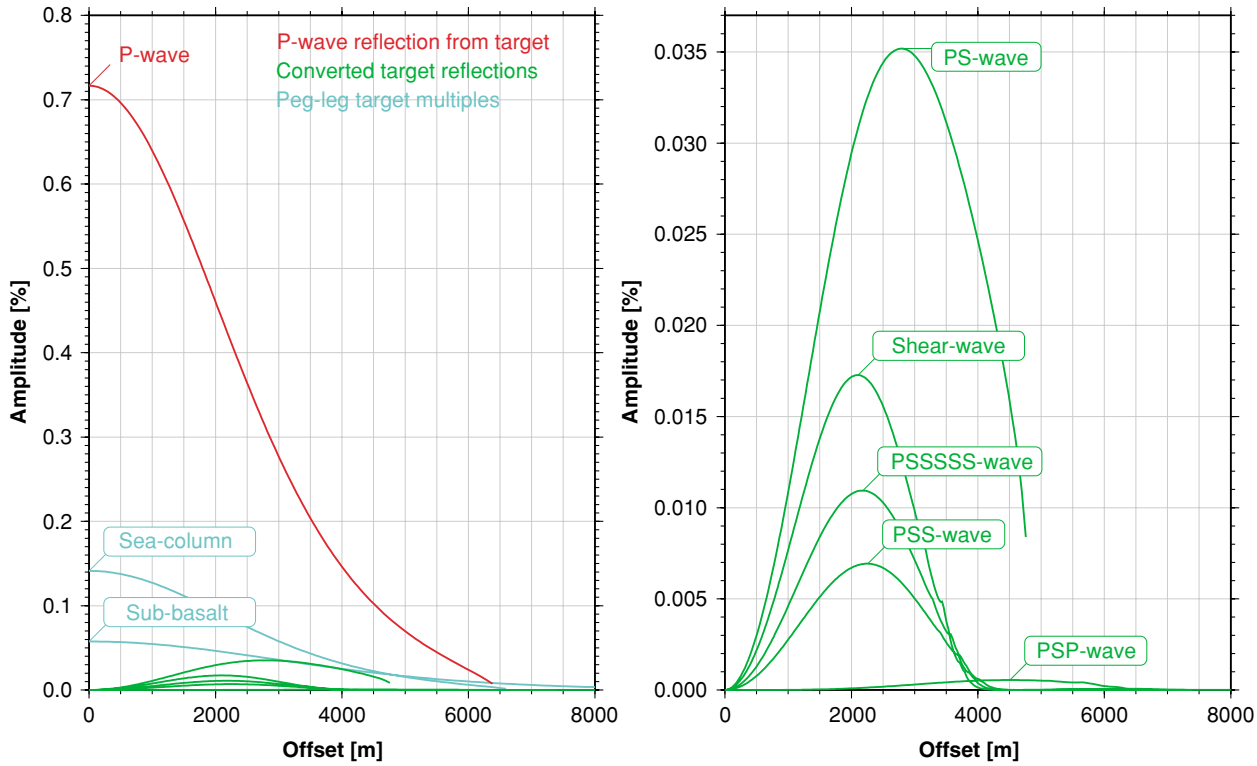

Figure 11 Left: effective reflection coefficients for the six strongest sub-basalt target reflections and two peg-leg multiples, based on the multilayered model of Fig. 8. Right: enlarged view of the expected amplitudes for converted modes.

Eni-Agip, BGS, BP, Chevron, CNPC, Conoco, Norsk-Hydro, Landmark, PetroChina, PGS, Phillips, Schlumberger, Texaco, Trade Partners UK and Veritas DGC.

REFERENCES

Aki K. and Richards P.G. 1980. *Quantitative Seismology – Theory and Methods*, Vol. 1. W.H. Freeman.

Frühn J., White R.S., Fliedner M., Richardson K.R., Cullen E., Latkiewicz C., Kirk W. and Smallwood J.R. 1998. Two-ship large aperture seismic profiles – application to imaging through basalt. 60th EAGE Conference, Leipzig, Germany, Extended Abstracts 1, 1–47.

Hanssen P., Li X.-Y. and Ziolkowski A. 2000. Converted waves for sub-basalt imaging? 70th SEG meeting, Calgary, Canada, Expanded Abstracts, MC 2.3.

Hanssen P., Ziolkowski A. and Li X.-Y. 1998. *Sub-basaltic imaging using converted shear-waves*. Transfer Report, Department of Geology and Geophysics, University of Edinburgh.

Hughes S., Barton P.J. and Harrison D. 1998. Exploration in the Shetland-Faeroe Basin using densely spaced arrays of ocean-bottom seismometers. *Geophysics* **63**, 490–501.

Jarchow C.M., Catchings R.D. and Lutter W.J. 1994. Large-explosive sources, wide-recording aperture, seismic profiling on the Columbia Plateau, Washington. *Geophysics* **59**, 259–271.

Kodaira S. *et al.* 1998. Structure of a volcanic continental margin derived from ocean-bottom seismographic data: the Northern Vøring Margin, off Norway. *Pure and Applied Geophysics* **152**, 1–21.

Li X.-Y. and MacBeth C.D. 1996. *Sub-basaltic imaging using converted shear-waves: a quantitative study*. Technical Report WL/96/09C, British Geological Survey.

Li X.-Y., MacBeth C., Hitchen K. and Hanssen P. 1998. Using converted shear-waves for imaging beneath basalt in deep water plays. 68th SEG meeting, New Orleans, USA, Expanded Abstracts, 1369–1372.

Longshaw S.K., Sunderland J. and Horn I. 1998. Mode conversion and multiples. 68th SEG meeting, New Orleans, USA, Expanded Abstracts, 1340–1342.

Pálmason G. 1965. Seismic refraction measurements of the basalt lavas of the Faeroe Islands. *Tectonophysics* **2**, 475–482.

Planke S., Alvestad E. and Eldholm O. 1999. Seismic characteristics of basalt extrusive and intrusive rocks. *The Leading Edge* **18**, 342–348.

Purnel G.W., McDonald J.A., Sekharan K.K. and Gardner G.H.F. 1990. Imaging beneath a high-velocity layer using converted waves. 60th SEG meeting, San Francisco, USA, Expanded Abstracts, 752–755.

Richardson K.R., White R.S., England R.W. and Fruehn J. 1999. Crustal structure east of the Faroe Islands: mapping sub-basalt sediments using wide-angle seismic data. *Petroleum Geoscience* **5**, 161–172.

Samson C., Barton P.J. and Karwatowski J. 1995. Imaging beneath an opaque basaltic layer using densely sampled wide-angle OBS data. *Geophysical Prospecting* **43**, 509–527.

Scrutton R.A. 1970. Results of a seismic refraction experiment on Rockall Bank. *Nature* **227**, 826–827.

Scrutton R.A. 1972. The crustal structure of Rockall Plateau microcontinent. *Geophysical Journal of the Royal Astronomical Society* **27**, 259–275.

Shipp R., Singh S. and Barton P. 1997. Sub-basalt imaging using full wavefield inversion. 67th SEG meeting, Dallas, USA, Expanded Abstracts, 1563–1566.

Stoker M.S., Hitchen K. and Graham C.C. 1993. The geology of the Hebrides and West Shetland shelves, and adjacent deep-water areas. In: *United Kingdom Offshore Regional Report*. HMSO, for the British Geological Survey.

Vilmann O., Gerstoft P. and Krenk S. 1998. *High-speed forward modelling applied in seismic data processing*. Ødegaard & Danneskiold-Samsøe ApS, Report 89.238/9, Final report Phase 1/2.

White R.S., Jones E.J.W., Hughes V.J. and Matthews D.H. 1982. Crustal structures from two-ship multichannel seismic profiles on the continental shelf off northwest Scotland. *Tectonophysics* **90**, 167–178.

Ziolkowski A., Hanssen P., Gatliff R., Jakubowicz H., Dobson A., Hampson G., Li X.-Y. and Liu E. 2003. Use of low frequencies for sub-basalt imaging. *Geophysical Prospecting* **51**, 169–182.